Journal of Materials Chemistry C

Accepted Manuscript

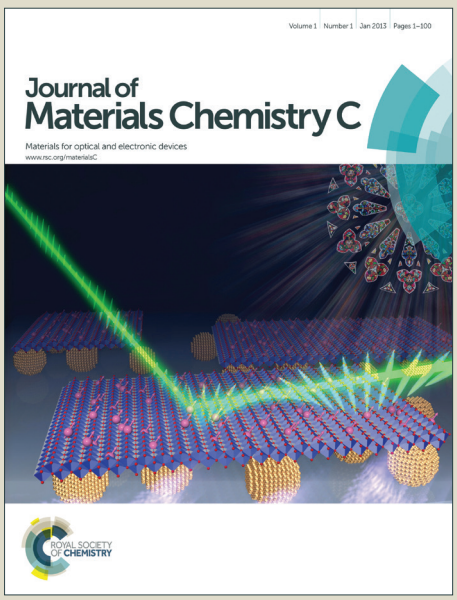

ROYAL SOCIETY OF CHEMISTRY

www.rsc.org/materialsC

Journal Name

RSCPublishing

ARTICLE

Weak intermolecular interactions promote blue luminescence of protonated 2,2'-dipyridylamine salts

Cite this: DOI: 10.1039/x0xx00000x

Received ooth January 2012,
Accepted ooth January 2012

DOI: 10.1039/x0xx00000x

www.rsc.org/

Alexander N. Chernyshev,[a,b] Dmitry Morozov,[a,c] Jarkko Mutanen,[d]

Vadim Yu. Kukushkin,[b] Gerrit Groenhof,*[,a,c] and Matti Haukka*[,a]

In this work we demonstrate that protonation and π-stacking can be exploited to convert non-luminescent 2,2'-dipyridylamine into blue-emitting derivatives. We have synthesized a series of luminescent 2,2'-dipyridylamine (dpa) salts, i.e., (dpaH)X•nSolv (dpa = 2,2'-dipyridylamine, X = HF_2, n = 0.5, Solv = H2O **1**; X = Cl, n = 2, Solv = H2O **2**; X = Br, n = 2, Solv = H_2O **3**; X = I n = 1, Solv = H_2O **4a**; X = I n = 1, Solv = $CHCl_3$ **4b**), $(dpaH)_2[SiF_6]$•H_2O **5** and (dpaH)X (X = I_3 **6**; SbF_6 **7**; BF_4 **8**) and characterized their emission properties, both in the solid-state and in solution. To rationalize our observations and relate the luminescence properties to the structure in the solid state and in solution, we have performed *ab initio* computations and showed that π-stacking interactions facilitate emission by sterically hindering radiation-less deactivation via a conical intersection. Our results thus not only provide a synthetic approach to cheap blue-emitting materials, but also revealed the essential role of weak intra- and intermolecular interactions, in particular hydrogen bonding and π-stacking, in the emission process. Our insights therefore provide new concepts for designing dpa-based systems with improved luminescence properties.

Introduction

Stable luminescent compounds emitting in the red, green, and blue parts of the spectrum are essential to create displays based on Organic Light Emitting Diodes (OLED).[1–4] Widespread application of OLED-based technology, however, is hindered by the limited availability of suitable blue-luminescent materials. Because of the large band gap required for blue emission, it is notoriously challenging to create compounds that are sufficiently stable towards photo-degradation.[5–11] Insofar as photo-degradation can be avoided to a large extent in the solid state, using crystalline materials may be a key to success. However, because of the common held belief that crystallization causes the luminescence of organic chromophores to quench,[12] most of today's OLEDs are based on amorphous materials and a lot of effort is focused on avoiding the formation of crystals.

Here, we show that protonation and ordered crystallization actually can turn the non-luminescent compound 2,2'-dipyridylamine (dpa, Chart 1) into an efficient blue-luminescent material (dpaH)X. Because of its large band-gap and commercial availability, the luminescent properties of various dpa derivatives and metal-organic frameworks have already received considerable attention.[13–26] However, all previous works have focused on the luminescent properties of complicated derivatives, inorganic complexes, and metal-organic frameworks of dpa. Instead, we have focused on one of the least complicated dpa systems, namely salts of protonated dpa with suitable anions.

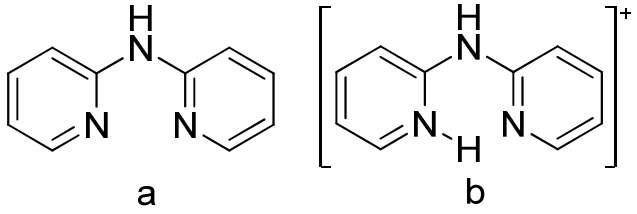

Chart 1. Dpa (a) and $(dpaH)^+$ (b).

In many of the luminescent dpa systems that have been studied previously, π-stacking was observed between the dpa units.[19–26] This is perhaps surprising, because chromophore stacking usually leads to efficient quenching, a phenomenon commonly referred to as Aggregation Caused Quenching (ACQ), and ACQ is usually rationalized by excimer formation.[12,27] Yet, in dpa derivatives, the stacking between the monomers seems to enhance, rather than suppress radiative decay. To explain this phenomenon in general terms, Tang and coworkers have proposed the concept of Aggregation Induced Emission (AIE),[28–30] in which aggregation facilitates emission, possibly by blocking competing non-radiative decay channels in the monomers. Nevertheless, the AIE concept has to the best of our knowledge not been invoked to explain the luminescence in dpa derivatives, nor has its mechanism been elucidated.

With the aims to reveal the mechanisms, by which stacking can cause emission in dpa, and to exploit this knowledge in creating cheap blue-luminescent materials, from which efficient

OLEDs can potentially be constructed, we have used a combination of experiment and computation to synthesize and characterize a series of dpa salts, namely (dpaH)X•nSolv (dpa = 2,2'-dipyridylamine, X = HF_2, n = 0.5, Solv = H2O **1**; X = Cl, n = 2, Solv = H2O **2**; X = Br, n = 2, Solv = H_2O **3**; X = I n = 1, Solv = H_2O **4a**; X = I n = 1, Solv = $CHCl_3$ **4b**), $(dpaH)_2[SiF_6]•H_2O$ **5** and (dpaH)X (X = I_3 **6**; SbF_6 **7**; BF_4 **8**). Our goal was to provide mechanistic insights into the luminescence of $(dpaH)^+$ and to study the possibilities of using these simple organic molecules as a source for emitting material.

Experimental

Materials and methods

Dpa, acids, and solvents used in syntheses were obtained from commercial sources (Aldrich, J. T. Baker, VWR, Merck) and used as received. Yields are based on dpa; isolated yields are given. Elemental analyses for carbon, hydrogen, and nitrogen were carried out with an Elementar Vario Micro apparatus and Elementar Vario EV III instrument. Electrospray ionization mass-spectra were obtained on a Bruker micrOTOF spectrometer equipped with electrospray ionization (ESI) source and MeOH was used as the solvent. The instrument was operated in positive ion mode using a *m/z* range of 50–3000. The capillary voltage of the ion source was set at −4500 V (ESI^+-MS) and the capillary exit at ±(70–150) V. In the isotopic pattern, the leftmost peak is reported. Infrared spectra were recorded on Bruker Alpha FT-IR spectrometer (4000–400 cm^{-1}) in powder form. ^1H and $^{13}C\{^1H\}$ NMR spectra were measured on a Bruker AV 300 instrument at ambient temperature. The absorption spectra were recordered on a Perkin Elmer Lambda 650 UV/VIS spectrophotometer. The excitation-emission matrices (EEMs) were measured with a custom made bispectrometer.[31–33] The light from a 450 W Xenon lamp (Oriel M-66923 housing, Newport corporation, Irvine, California and Osram XBO 450 W bulb, Osram AG, Winterthur, Switzerland) was directed to the sample through a Czerny-Turner monochromator (DTMc300, Bentham Instruments Ltd, Berkshire, United Kingdom). The used band width and sampling interval of the excitation light were both 5 nm. The emitted light was collected with a lens to an optical fiber attached to a spectrograph detector (PMA-12, Hamamatsu Photonics K.K., Japan). The spectrograph operates at the wavelength range 200–950 nm with 0.72–0.76 nm spectral sampling. In the used measurement, geometry angle of incidence was 0° and detection angle was 45°. The emission spectra of the solutions were measured on a Perkin Elmer LS 55 spectrofluorimeter. The relative fluorescence quantum yield was measured using 9,10-diphenylanthracene in cyclohexane as a standard reference.[34] Time resolved fluorescence measurements were performed with a PicoQuant HydraHarp 400 time correlated single photon counting data acquisition system with 375 nm pulsed diode laser.

X-ray structure determinations

The crystals of **1**, **2**, **3**, **4a**, **4b**, **5**, **6**, and **8** were obtained by a slow evaporation of solvents at 4–5 °C. Crystals were immersed in cryo-oil, mounted in a MiTeGen loop, and measured at a temperature of 100 K (**1**, **4a**, **8**) or 170 K (**3**, **4b**, **5**, **6**). In addition, in order to compare the structures of the luminescent materials at low and ambient temperatures the crystals of **2**, **4b**, and **5** were also measured at 290 K. We were not able to obtain high quality X-ray data of **1** and **8** at 290 K. Crystal structure of **2** at 150 K and of **3** and **4a** at 293 K are previously reported by other groups.[35,36] The X-ray diffraction data were collected on a Nonius KappaCCD, Bruker Axs KappaApexII or Agilent SuperNova diffractometers using Mo Kα radiation (λ = 0.71073 Å) or Cu Kα radiation (λ = 1.54184 Å). The *Apex2*,[37] *EvalCCD*[38] and *Denzo/Scalepack*[39] program packages were used for cell refinements and data reductions. The structures were solved by direct methods using *Shelxs 97*[40] or *SUPERFLIP*[41] program with the *Olex 2*[42] graphical user interface. A semi-empirical or numerical absorption correction (*SADABS*[43] or *Xprep in Shelxtl*[44]) was applied to all data. Structural refinements were carried out using *SHELXL-97*, *SHELXL-2013*, or *SHELXL-2014*.[40]

Structure **1** is expected to contain bifluoride ions based on the planar geometry of HF_2^- and the lengths of the H–F bonds (1.147–1.156 Å) that correspond to those reported in the literature.[45] Synthetic methodology also support the composition of **1**. Structures of **2** and **3** were solved in a chiral space group Cc. Attempts to solve these structures in centro-symmetric space group C2/c lead to unsatisfactory results. However, structure **2** was refined as inversion twin with the BASF value refined to 0.45833.

The structures of **4b**, **5**, **6**, and **8** were solved in a centrosymmetric space groups Pnma, P $\bar{1}$, P $\bar{1}$, and $P2_1/c$ respectively. In **4b**, the bridging amine nitrogen was disordered over two alternative sites around the center of symmetry with equal occupancies. The crystal of **6** was found to be twinned via a 179.8° rotation about the reciprocal axis (1, 0, 1). The two components were determined using the program CELL_NOW,[46] integrated using *Apex2* program package, merged and corrected for absorption using *TWINABS*.[47] In the structure of **8**, the fluorine atoms F(1)–F(4) of the anion are disordered over two sites with occupancies of 0.64:0.36.

All NH hydrogen atoms in the structures of **2**, **3**, **4a** and the pyridine NH hydrogen atom in the structure of **8** were located from the difference Fourier map and refined isotropically, whereas the pyridine NH hydrogen atoms in the structures of **5** both at 170 K and 290 K were located from the difference Fourier map but constrained to ride on their parent atom. In the structures of **2**, **5**, and **8**, the optimal position for the hydrogen atom was in the center (for **5**) or close to the center (for **2** and **8**) of neighboring pyridyl nitrogens. This, in turn, led to overestimated N–H distances. However, we did not constrain these N–H bonds since these hydrogen atoms are involved in strong intermolecular hydrogen bonds having a resonance-assisted nature. All the H_2O and HF_2^- hydrogen atoms were located from the difference Fourier map but constrained to ride on their parent atom, with $U_{iso} = 1.5U_{eq}$. Other hydrogen atoms

were positioned geometrically and constrained to ride on their parent atoms, with C–H = 0.93–0.95 Å, N–H = 0.86–0.88 Å, and U_{iso} = 1.2–1.5 U_{eq} (parent atom). The crystal structures and crystallographic details are given in Figures S1–S10 and Table S1 (ESI†).

Synthetic work

2,2'-Dipyridylamine (dpa) (1.46 mmol, 250 mg) was suspended in water (5 mL) and appropriate acid was added (for **1** 2.92 mmol, 130.4 µL 40% HF in water, lower amount of this acid leads to incomplete reaction and residues of unreacted dpa in the system, reaction was carried out in a plastic flask; for **2** 1.46 mmol, 121.6 µL 37% HCl in water; for **3** 1.46 mmol, 166.2 µL 48% HBr in water; for **4a** 1.46 mmol, 192.8 µL 57% HI in water; for **5** 7.3 mmol, 326 µL 40% HF in water, reaction was carried out in a glass flask; for **6** excess (3 mL) of 57% HI in water; for **7** 1.46 mmol, 503.6 mg $HSbF_6$•$6H_2O$, for **8** 1.46 mmol, 233.7 µL 85% HBF_4•OEt_2). The reaction mixture was stirred for 1 h and left to stand for 8 h. The released precipitate (colorless solution in case of **1** without precipitate, colorless solutions with white-off precipitate in cases of **2**, **3**, **5**, **7**, and **8**, yellow solution with brownish precipitate in cases of **4a** and **6**) was dried under vacuum at RT and recrystallized from methanol (yields: 289 mg, 90% (**1**), 338 mg, 95% (**2**), 400 mg, 95% (**3**), 398 mg, 86% (**4a**), 332 mg, 90% (**5**), 746 mg, 92% (**6**), 356 mg, 94% (**7**), 693 mg, 92% (**8**). **4b** was obtained by recrystallization of **4a** from boiling chloroform, yield 97%.

(dpaH)[HF_2]•0.5H_2O (1). Found: C 54.70; H 5.29; N 19.23 (Calcd. for $C_{10}H_{12}N_3F_2O_{0.5}$: C 54.54; H 5.49; N 19.08). ESI^+-MS, *m/z*: 172.0890 $[dpaH]^+$. IR spectrum (selected bands, cm^{-1}): 3390 m, 3364 m *ν*(N–H and C–H); 2955 w *ν*(N–H); 1669 s, 1604 s *ν*(C=N or C=C); 1521 s *ν*(C=N or C=C); 1313 w, 1255 m *ν*(C–N); 1147 w, 830 w, 778 m *δ*(C–H_{Py}). ^1H NMR spectrum (CD_3OD, *δ*): 8.23 (d, 7.0 Hz, 2H), 7.82 (t, 7.0 Hz, 2H), 7.43 (d, 7.0 Hz, 2H), and 7.04 (t, 7.0 Hz, 2H). $^{13}C\{^1H\}$ NMR spectrum (CD_3OD, *δ*): 154.5 (C_{ipso}), 145.3, 141.1, 118.2, and 114.4 (C_{Py}).

(dpaH)Cl•2H_2O (2). Found: C, 49.38; H, 5.67; N, 17.19 (Calcd. for $C_{10}H_{14}N_3ClO_2$: C, 49.29; H, 5.79; N, 17.24). ESI^+-MS, *m/z*: 172.0890 $[dpaH]^+$. IR spectrum (selected bands, cm^{-1}): 3341 s *ν*(N–H or C–H); 2946 w *ν*(N–H); 1660 s, 1593 s *ν*(C=N or C=C); 1504 s *ν*(C=N or C=C); 1246 m *ν*(C–N); 1148 w, 842 w, 774 m *δ*(C–H_{Py}). ^1H NMR spectrum (CD_3OD, *δ*): 8.45 (d, 7.4 Hz, 2H), 8.13 (t, 7.4 Hz, 2H), 7.39 (d, 7.4 Hz, 2H), and 7.32 (t, 2H, 7.4 Hz). $^{13}C\{^1H\}$ NMR spectrum (CD_3OD, *δ*): 153.2 (C_{ipso}), 143.6, 142.3, 119.3, and 115.6 (C_{Py}).

(dpaH)Br•2H_2O (3). Found: C, 41.59; H, 4.95; N, 14.52 (Calcd. for $C_{10}H_{14}N_3BrO_2$: C, 41.68; H, 4.90; N, 14.58). ESI^+-MS, *m/z*: 172.0890 $[dpaH]^+$. IR spectrum (selected bands, cm^{-1}): 3384 m, 3335 m *ν*(N–H and C–H); 2960 w *ν*(N–H); 1655 s, 1591 s *ν*(C=N or C=C); 1502 s *ν*(C=N or C=C); 1311 w, 1270 m *ν*(C–N); 1140 w, 842 w, 761 m *δ*(C–H_{Py}). ^1H NMR spectrum (CD_3OD, *δ*): 8.35 (d, 6.8 Hz, 2H), 7.95 (t, 6.8 Hz, 2H), 7.45 (d, 6.8 Hz, 2H), and 7.16 (t, 2H, 6.8 Hz). $^{13}C\{^1H\}$ NMR spectrum (CD_3OD, *δ*): 154.1 (C_{ipso}), 144.7, 141.7, 118.5, and 114.6 (C_{Py}).

(dpaH)I•H2O (4a). Found: C, 37.77; H, 3.82; N, 13.16 (Calcd. for $C_{10}H_{12}N_3IO$: C, 37.87; H, 3.81 N, 13.25). ESI^+-MS, *m/z*: 172.0890 $[dpaH]^+$. IR spectrum (selected bands, cm^{-1}): 3414 m, 3385 m *ν*(N–H and C–H); 2991 w *ν*(N–H); 1660 s, 1602 s *ν*(C=N or C=C); 1510 s *ν*(C=N or C=C); 1304 w, 1267 m *ν*(C–N); 1147 w, 842 w, 776 m *δ*(C–H_{Py}). ^1H NMR spectrum (CD_3OD, *δ*): 8.37 (d, 7.2 Hz, 2H), 8.00 (t, 7.2 Hz, 2H), 7.37 (d, 7.2 Hz, 2H), and 7.20 (t, 2H, 7.2 Hz). $^{13}C\{^1H\}$ NMR spectrum (CD_3OD, δ): 153.6 (C_{ipso}), 143.6, 142.5, 118.8, and 114.9 (C_{Py})

(dpaH)I•$CHCl_3$ (4b). Found: C, 37.77; H, 3.82; N, 13.16 (Calcd. for $C_{10}H_{12}N_3IO$: C, 37.87; H, 3.81 N, 13.25). ESI^+-MS, IR spectrum, ^1H and $^{13}C\{^1H\}$ NMR spectra (CD_3OD) are the same as for **4a** besides the additional resonance due to $CHCl_3$.

(dpaH)$_2$[SiF_6]•H_2O (5). Found: C, 47.50; H, 4.52; N, 16.58 (Calcd. for $C_{20}H_{22}N_6F_6OSi$: C, 47.61; H, 4.40 N, 16.66). ESI^+-MS, *m/z*: 172.0890 $[dpaH]^+$. IR spectrum (selected bands, cm^{-1}): 3425 m, 3390 m *ν*(N–H and C–H); 2990 w *ν*(N–H); 1676 s, 1614 s *ν*(C=N or C=C); 1511 s *ν*(C=N or C=C); 1312 w, 1283 m *ν*(C–N); 1164 w, 790 m *δ*(C–H_{Py}). ^1H NMR spectrum (CD_3OD, *δ*): 8.32 (d, 7.1 Hz, 2H), 7.93 (t, 7.1 Hz, 2H), 7.45 (d, 7.1 Hz, 2H), and 7.14 (t, 2H, 7.1 Hz). $^{13}C\{^1H\}$ NMR spectrum (CD_3OD, *δ*): 154.1 (C_{ipso}), 144.3, 141.9, 118.6, and 114.9 (C_{Py}).

(dpaH)[I_3] (6). Found: C, 21.76; H, 1.84; N, 7.67 (Calcd. for $C_{10}H_{10}N_3I_3$: C, 21.72; H, 1.82 N, 7.60). ESI^+-MS, *m/z*: 172.0890 $[dpaH]^+$. IR spectrum (selected bands, cm^{-1}): 3413 m, 3398 m *ν*(N–H and C–H); 2981 w *ν*(N–H); 1646 s, 1598 s *ν*(C=N or C=C); 1446 s *ν*(C=N or C=C); 1235 m *ν*(C–N); 1157 m, 1147 m, 764 s *δ*(C–H_{Py}). ^1H NMR spectrum (CD_3OD, *δ*): 8.40 (d, 6.4 Hz, 2H), 8.10 (t, 6.4 Hz, 2H), and 7.29 (m, 4H). $^{13}C\{^1H\}$ NMR spectrum (CD_3OD, *δ*): 153.1 (C_{ipso}), 143.5, 142.3, 119.2, and 115.4 (C_{Py}).

(dpaH)[SbF_6] (7). Found: C, 29.36; H, 2.54; N, 10.21 (Calcd. for $C_{10}H_{10}N_3F_6Sb$: C, 29.44; H, 2.47 N, 10.30). ESI^+-MS, *m/z*: 172.0890 $[dpaH]^+$. IR spectrum (selected bands, cm^{-1}): 3447 m, 3332 m *ν*(N–H and C–H); 2995 w *ν*(N–H); 1656 s, 1605 s *ν*(C=N or C=C); 1504 s ν(C=N or C=C); 1245 m *ν*(C–N); 1153 w, 864 w, 766 m *δ*(C–H_{Py}). ^1H NMR spectrum ((CD_3)$_2$SO, *δ*): 11.62 (s, br, 1H, NH_{amine}) 8.40 (d, 6.5 Hz, 2H), 8.09 (t, 6.5 Hz, 2H), 7.34 (d, 6.5 Hz, 2H), 7.27 (t, 2H, 6.5 Hz), and 4.06 (s, br, 1H, NH_{Py}). $^{13}C\{^1H\}$ NMR spectrum ((CD_3)$_2$SO, *δ*): 151.4 (C_{ipso}), 142.8, 141.9, 117.7, and 114.1 (C_{Py}).

(dpaH)[BF_4] (8). Found: C, 46.29; H, 3.97; N, 16.32 (Calcd. for $C_{10}H_{10}N_3BF_4$: C, 46.37; H, 3.89 N, 16.22). ESI^+-MS, *m/z*: 172.0890 $[dpaH]^+$. IR spectrum (selected bands, cm^{-1}): 3329 m *ν*(N–H or C–H); 2998 w *ν*(N–H); 1656 s, 1607 s *ν*(C=N or C=C); 1504 s *ν*(C=N or C=C); 1308 w, 1246 m *ν*(C–N); 1158 w, 846 w, 764 s *δ*(C–H_{Py}). ^1H NMR spectrum (CD_3OD, *δ*): 8.38 (d, 8.1 Hz, 2H), 8.07 (t, 8.1 Hz, 2H), and 7.26 (m, 4H). $^{13}C\{^1H\}$ NMR spectrum (CD_3OD, δ): 153.0 (C_{ipso}), 143.5, 142.1, 119.2, and 115.3 (C_{Py}).

Computational details.

The ground state equilibrium geometry of compound **3** was optimized at the PBE0/cc-pVDZ level of theory.[48] Initial geometry was taken from the crystal structure of 3. Stationary points on the potential energy surface of the first electronic singlet excited state as well as the minimum energy conical intersection (MECI) between the ground and excited state were

optimized at the state-averaged (over 2 states) SA(2)-CASSCF(14,13)/cc-pVDZ level of theory, including all π-electrons and π-orbitals. Vertical excitation energies, used to determine absorption and emission wavelengths were obtained with the XMCQDPT2/SA(4)-CASSCF(14,13)/cc-pVDZ[49] approach using an active space that include all molecular orbitals of the π-type. Relaxation pathways connecting the stationary states were obtained by relaxed scans using SA(2)-CASSCF(14,13)/cc-pVDZ level of theory separately for ground and excited states (also XMCQDPT2 corrections were calculated for optimized geometries), whereas the pathway to the MECI was obtained by linearly interpolating the internal coordinates. Dimer calculations were performed at SA(4)-CASSCF(16,14)/cc-pVDZ level on dimer structures taken from the X-ray structures of **3** and **8**. The hydrogen positions in these dimers were optimized using PBE0/cc-pVDZ. The active space of the dimer consisted of 8 electrons and 7 π-orbitals on each monomer, yielding the aforementioned active space of 16 electrons in 14 orbitals. The polarizable continuum model was used to include effect of solvent in our computations.[50] For all electronic structure calculations the Firefly version 8.0 package,[51] partially based on the GAMESS (US) source code,[52] was used.

Results and discussion

In the present work, we have synthesized and analyzed photophysical properties of a series of new luminescent compounds i.e. different salts of monoprotonated 2,2'-dipyridylamine $(dpaH)^+$ with all four halides as well as BF_4^-, SiF_6^{2-}, and SbF_6^- as counterions. The single-crystal X-ray structures showed that in all cases the $(dpaH)^+$ cations are planar and contain intramolecular hydrogen bonds between the hydrogen of protonated pyridyl nitrogen and non-protonated pyridyl nitrogen as expected (Figure 1).[35,53]

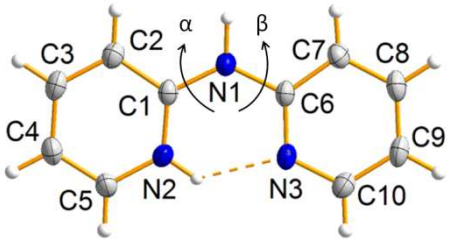

Figure 1. The molecular structure of $(dpaH)^+$ cation in **2**. The counter anion (Cl^-) and water of crystallization have been omitted for clarity. The thermal ellipsoids are drawn at the 50% probability level. Two torsion angels represent rotation around protonated (α) and deprotonated (β) rings.

This intramolecular hydrogen bond, which can be classified as a positive charge assisted hydrogen bond in some cases,[54–57] hinders twisting of the pyridyl rings leading to a planar conformation of $(dpaH)^+$. The planar monomers are packed face-to-face via intermolecular π-stacking interactions, supported by hydrogen bonds involving the amine NH and the anion for **6** and **8**, and in addition solvent of crystallization for **1**–**4a** and **5** (Figure 2 for **3**, Figures S11 – S15 in ESI† for **1**, **2**, **4a**, **5** and **6**). The structure of **8** also contains anion-π interactions (Figure S16 in ESI†). Structure of **4b** does not contain any considerable face-to-face stacking, but the twisting of $(dpaH)^+$ is nevertheless restricted by the set of weak interactions (Figure 7 and discussion below).

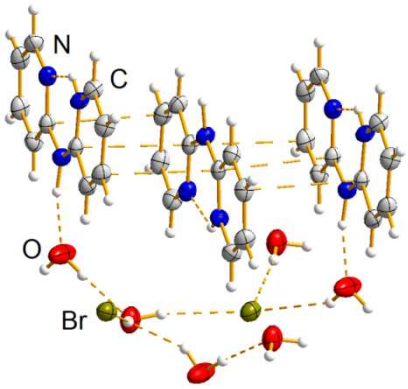

Figure 2. The π-stacking interactions, supported by hydrogen bonds involving the amine NH, Br^-, and water of crystallization in the structure of $(dpaH)Br•2H_2O$ (**3**).

We were not able to obtain the X-ray structure of compound **7**, but as its emission and absorption properties are similar to those of **1**–**3**, **5**, and **8** both in the solid state and in solution, we believe that it also exhibits π-stacking interactions between the $(dpaH)^+$ units.

Solid state luminescence of dpa salts.

Under irradiation with UV light, crystals of **1**, **2**, **3**, **4b**, **5**, **7**, and **8** emit blue light, while crystals of **4a** and **6** are not emissive (Table 1). The highest intensity luminescence was obtained with crystals of **8**, as shown in Table 1. The excitation-emission matrix (EEM) of **8** is shown on the Figure 3, while the EEMs of **1** – **3**, **4b**, **5** and **7** are shown on the Figures S17 – S22 in ESI†. Unlike $(dpaH)^+$, crystals of unprotonated dpa, crystallized in three different polymorphic forms[58], were not luminescent, demonstrating that protonation is essential for luminescence.

Table 1. Emission properties of the dpa salts in the solid state.

Compound	Emission maximum position, nm	Emission maximum intensity, arbitrary units	Excitation wavelength corresponding to emission maximum, nm	Fluorescence lifetime, ns
1	424	4.3	374	23.3
2	408	8.4	376	5.8
3	404	5.7	372	2.7
5	444	5.6	368	25.3
4b	≈485	1.3*	360–400	–
7	418	7.1	364	22.0
8	406	10.1	366	7.0

*Because **4b** is much less emissive than **1**–**3**, **5**, **7**, and **8** we were not able to measure its emission with the same exposure time, so the emission maximum intensity of **4b** is not comparable with intensity maxima of **1**–**3**, **5**, **7**, and **8**. Due to the same reason the emission lifetime of 4b was not determined.

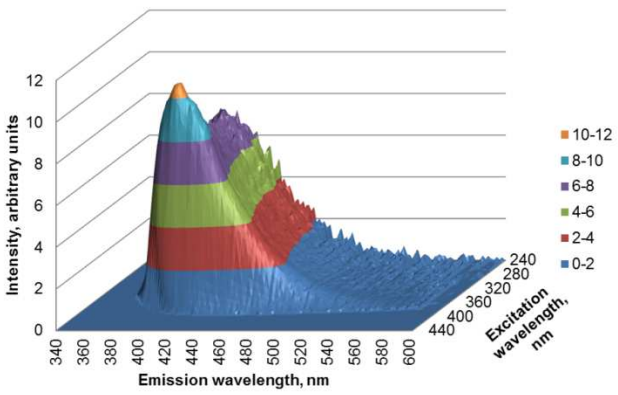

Figure 3. Excitation-emission matrix (EEM) of solid (dpaH)[BF_4] (8).

In $(dpaH)^+$, the pyridyl rings are locked in planar arrangement, which is expected to hinder the radiation-less deactivation though rotation of the rings. The planarity is further supported by the π-stacking of the $(dpaH)^+$ cations.

Another option for the origin of emission in systems of stacked molecules is excimer/exciplex formation as in the case of pyrene.[59] This is possible even if π-stacking typically causes quenching in aggregates. However, in our system, the excimer/exciplex mechanism was found not to play a role in emission processes (see the computational section for details).

Computed absorption and emission spectra.

To establish the mechanism by which the $(dpaH)^+$ salts emit in crystals, we have performed *ab initio* quantum chemistry calculations. We computed the (i) absorption and emission spectra of a $(dpaH)^+$ monomer and stacked dimers (as a model for the crystal), and (ii) radiation-less deactivation (*i.*e., quenching) pathways of the $(dpaH)^+$ monomer. In our calculations of the monomer, we consider two rotameric conformations **a**, with an intramolecular hydrogen bond between the pyridyl rings, and **b**, without the hydrogen bond (Table 2, top).

Table 2. Calculated vertical excitation energies of the $(dpaH)^+$ monomer in the two conformations and the stacked dimer.

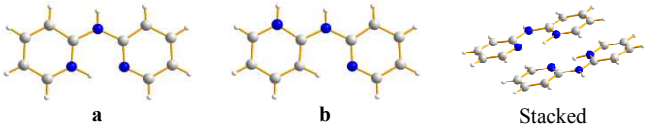

a			**b**			Stacked		
Transition	E, eV	E, nm	Transition	E, eV	E, nm	Transition	E, eV	E, nm
S0->S1	3.91	316	S0->S1	3.75	331	S0->S1	3.59	345
S0->S2	4.63	267	S0->S2	4.78	259	S0->S2	3.73	332
S0->S3	5.36	231	S0->S3	5.41	229	S0->S3	4.83	256
-	-	-	-			S0->S4	5.03	246
S1->S0*	3.06	405	S1->S0*	2.77	448	–	–	–

* emission

Vertical excitation energies were calculated at the XMCQDPT2/SA(4)-CASSCF(14,13)/cc-pVDZ level of theory for the three lowest energy π–π* transitions in the **a** and **b** conformations of the monomer and are listed in Table 2. Including the effect of chloroform solvent, using the PCM solvent model, causes a 1 nm shift in absorption wavelength. Because this difference is so small, we have performed all further calculations in gas-phase. Furthermore, the counterions were not considered, as preliminary tests at the TD-DFT level indicated that including these anions do not shift the absorptions significantly. On the other hand, counterions can play a role in stabilization of excited state and thus affect emission spectra and lifetimes. However, including the counter ions in the geometry optimization in the excited state, which is required for computing the emission wavelength, is beyond the capabilities of our computational resources.

The four lowest energy excitations in the dimer, calculated at the XMCQDPT2/SA(4)-CASSCF(16,14)/cc-pVDZ level are localized on the monomers. These excitations are listed in the third column of Table 2 for the dimer structure taken from the crystal structure of **3**. Changing the stacking mode of the dimer to that observed in the crystal structure of **8** (Figure S23 in ESI†) does not affect the character of these excitations (Table S3 in ESI†). Although stacking causes a differential red shift for both monomers, we did not find evidence for shared or excitonic transitions. We will later use this differential red shift as a fingerprint to identify stacking in solution.

For the two conformers of the $(dpaH)^+$ monomer (**a** and **b**) we also calculated the emission energy after relaxing the geometry in the first excited state (S1). For conformer **a** the calculated emission at 405 nm is in reasonable agreement with the measured emission of most crystals (Table 1). We speculate that deviations are due to differences in the crystal packing and interactions with counterions. The most significant deviation was found for the crystal of **5**. Although the emission maximum of crystal **5** (444 nm, Table 1) matches nicely the emission computed for the **b** conformation (448 nm, Table 2), inspection of the crystal structure rules out the possibility that the $(dpaH)^+$ monomers in crystal of **5** adopt the **b** conformation. Interestingly, we found that in this crystal the proton is located in between the pyridyl nitrogen atoms (Figures S7–S8, ESI†), which is reminiscent of the so-called short strong hydrogen bond.[60,61] In our model system, however, the ground-state barrier for proton transfer between the rings was 2.71 kJ/mol, which is too far above the zero-point energy for the proton to be shared. Addressing this issue, and the effect of the shared proton on the absorption and emission spectra would require a more sophisticated representation of the crystal environment, including the counter ions and water molecules, in our *ab initio* computations, and is therefore beyond the scope of this work.

To determine whether the stacking or the intramolecular hydrogen bond enhances luminescence by hindering radiation-less decay, we searched for deactivation pathways that connect the Frank-Condon region to a conical intersection in the monomer. Based on dpa's topology we studied two pathways. The first involves rotation of the unprotonated pyridyl ring

(torsion α in Figure 1), whereas the second pathway involves rotation of the protonated ring (torsion β). The energy profiles obtained by performing a relaxed scan of the torsion angle in the first excited state are shown in Figures 4 and 5 for both rotations. The upper panels (A) display the energy at the CASSCF level, while the lower panels (B) show the energy at the XMCQDPT2 level. For the ground state PBE0 level of theory was also used. Comparing the profiles, we observe that twisting the protonated ring is a barrierless process at the CASSCF level of theory, whereas twisting the unprotonated ring is not. Therefore, the initial relaxation after photo-excitation of the isolated $(dpaH)^+$ monomer involves twisting of the protonated ring. Furthermore, although the intramolecular hydrogen bonding stabilizes the planar structure of $(dpaH)^+$ in the ground state (for comparison, the neutral dpa is non-planar, see Figure S24), it does not prevent the twisting in the excited state. Thus, the effect of the hydrogen bond alone is not sufficient for the emission. From the ground state relaxed scans we can also conclude that conformer **a** is more stable on the ground state than conformer **b** by ca. 10 kcal/mol. In the excited state, this difference is smaller (~5 kcal/mol).

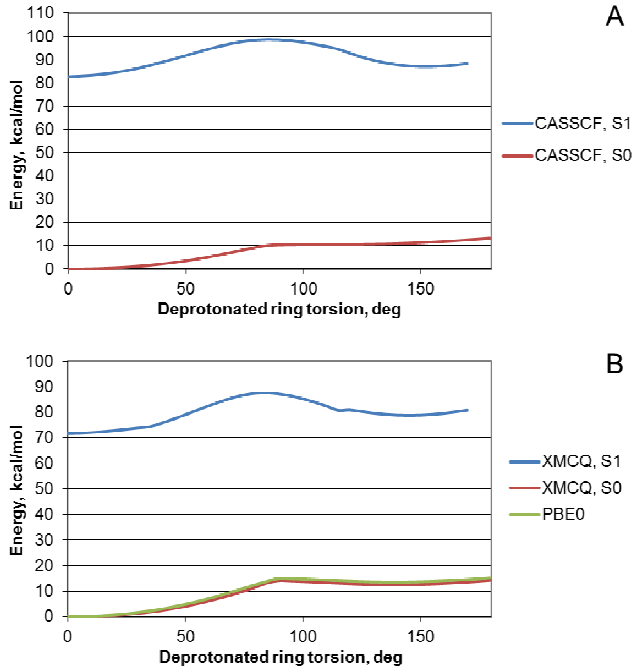

Figure 4. The energy profiles for the rotation of deprotonated pyridyl ring (A – CASSCF level, B – XMCQDPT2 level).

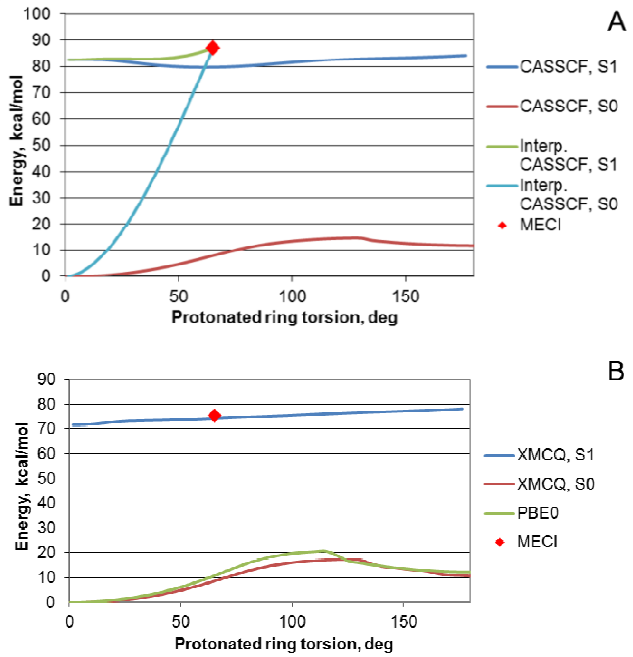

Figure 5. The energy profiles for the rotation of protonated pyridyl ring (A – CASSCF level, B – XMCQDPT2 level) and the Franck-Condon point.

We located a conical intersection near the twisted minimum that is about 3 kcal/mol higher in energy than the Franck-Condon point (dot in Figure 5). The geometry of this conical intersection is shown in Figure 6. In addition to a twist of 65 degrees of the protonated ring, the configuration of the nitrogen in this ring was changed from a planar sp^2 to a tetrahedral sp^3 configuration. Interpolating between the Franck-Condon point and this conical intersection did not reveal a barrier. Therefore, we assume that the isolated $(dpaH)^+$ can deactivate efficiently via this intersection. In contrast, the tight stacking of the monomers in crystals **1**–**3**, **5**, **7**, and **8** hinder rotation and therefore enhance luminescence. Although after the XMCQDPT2 corrections, the S1 minimum disappears, the conical intersection remains within 4 kcal/mol of minimum (Figure 5b). Because we recomputed the energies along the CASSCF minimum energy pathway, rather than re-optimized the pathway at the XMCQDPT2 level, the error in the profiles is typically in the order of the energy difference between CASCCF and XMCQDPT, which can be several kcal/mol

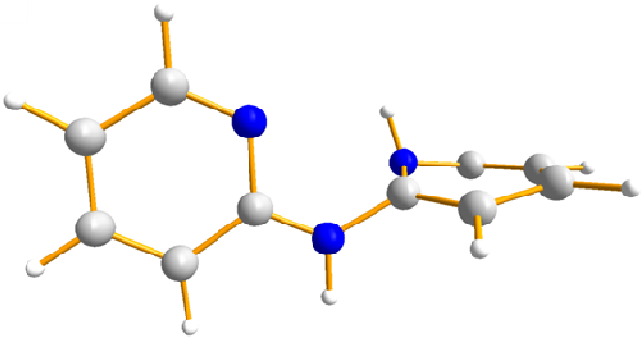

Figure 6. Geometry of the conical intersection.

The assembly of the $(dpaH)^+$ cations in structure **4b** differs from the other structures as no considerable face-to-face π-stacking was observed in the crystal (Figure 7). However, despite the lack of π-stacking, crystals of **4b** are luminescent, albeit with a much lower efficiency (Table 1). A closer analysis of the crystal structure revealed that the $(dpaH)^+$ cations are locked in a different way. In **4b**, each $(dpaH)^+$ unit is connected to the adjacent cations by the face-to-face π-π interactions with large offsets and with face-to-edge CH–π interactions. This leads to formation of square opening channels filled with chloroform of crystallization. The channel structure prevents the twisting of the rings and activate the molecule for luminescence. However, the packing is less restricted compared to the true face-to-face π-stacked systems and therefore **4b** possesses much weaker emission than crystals of **1**–**3**, **5**, **7**, and **8**.

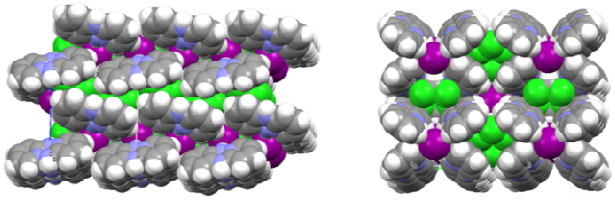

Figure 7. Spacefill view of crystal structure of 4b at 290 K from *b* and *a* crystallographic axes

The lack of luminescence in crystals **4a** and **6** is less obvious since in these crystals the cations are stacked at least to some extent. However, in contrast to the other crystals, stacking in the crystal of **4a** is restricted to dimers leading to a much less constrained system that we assume is not rigid enough to completely prevent the twisting of the rings. To explain the absence of emission in crystals of **6** we speculate that the luminescence is efficiently quenched by excitation energy transfer to the I_3^- anions, which are ordered in chains that run parallel to the $(dpaH)^+$ stacks throughout the crystal. The quenching role of I_3^- is supported by the observation that the absorption spectrum of I_3^- overlaps with the emission spectrum of $(dpaH)^+$. Alternatively, the quenching of the luminesce in the crystals of **4a** and **6** may also be due to the heavy atom effect of I^-, which was recently reported for tetraphenylethene derivatives.[62]

Summarizing, the results of the computations suggest that the hydrogen bond alone is not sufficient to block radiation-less deactivation, but it aids in maintaining a planar geometry (Figures S1–S10, ESI†), which facilitates stacking. This stacking, however, does not promote exciplex formation, because the excitation is always localized on single monomer. Instead, the stacking hinders the internal twisting of the monomers, which is required for radiation-less decay through the conical intersection. By blocking the latter pathway, the stacking enhances emissive decay instead. Thus, we conclude that in crystals of the protonated dpa salts, AIE is responsible for luminescence, and that, in contrast to the previous assumptions, π-stacking does not need to be avoided in AIE.[28,29]

Emission and absorption of dpa salts in solutions.

Based on our calculations, we anticipate that in solution, radiation-less deactivation competes strongly with emission. Furthermore, because radiation-less decay requires a significant rotation of the protonated pyridyl ring, we also expect the efficiency to decrease when we increase the viscosity of the solvent. To validate these hypotheses, we have measured the emission of the $(dpaH)^+$ salts in different solvents. We have used poor solvating (chloroform) and good solvating solvents (n-alcohols) and varied the viscosity of the latter by increasing the alkane length in a series of alcohols ROH (R = CH_3, n-C_4H_9, n-C_5H_{11}, n-C_6H_{13}, n-C_7H_{15}, n-C_9H_{19}, n-$C_{11}H_{23}$). The reason for using a solvent with the low solvation ability is to investigate if it can promote aggregation and therefore luminescence.

Indeed, the emission depends on the choice of solvent. In methanol, which has a high solvation ability, irradiation with UV light (λ_{ex} = 368 nm) does not incude emission in any of the dpa salts, whereas in chloroform, which is a poorer solvent, **1**, **2**, **3**, **5**, **7**, and **8** are luminescent (in Table 3 and Figure 8 the emission properties of chloroform solutions of dpa salts are presented. We have not included the data of the methanol solutions, because we could not observe emission from these solutions.). Because of the strong overlap of the I_3^- and $(dpaH)^+$ absorption and emission spectra and the possibility of EET (see above), we do not consider **6** in our analysis. The emission spectra of the dpa salts in chloroform are broad, and in some cases the peaks in the spectrum exhibit shoulders. Comparison between these spectra and the calculated emission maxima of **a** and **b** conformers of $(dpaH)^+$ (Table 2), suggests that **a** and **b** can interconvert in solution.

Table 3. Emission properties of chloroform solutions of the dpa salts.

Substance	C•10^{-4}, M	λ_{max}	E_{max}	Φ, %	τ, ps
1	5	433	131.9	5	720
2	5	431	560	12	650
3	5	429	235.7	9	710
4	5	–	0	0	–
5	1.25	434	251.1	11	750
6	2.5	–	0	0	–
7	2.5	399	107.8	8	720
8	2.5	429	40.8	7	720

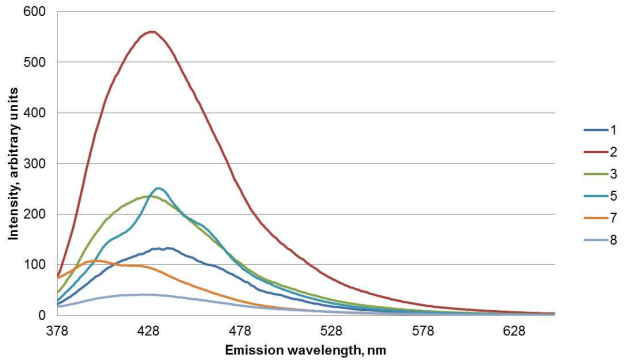

Figure 8. Emission spectra of chloroform solutions of dpa salts

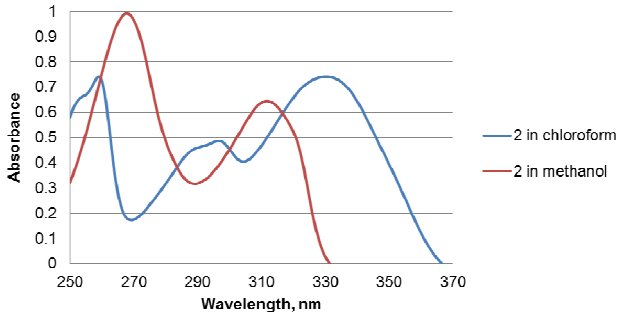

Figure 9. Absorption spectra of 2 in chloroform and methanol (C = 5•10^{-4} M).

In methanol, two major absorption peaks were observed at 264 nm and 311 nm (Figure 9). Based on our calculations (Table 2), we assign these two peaks to conformer **a**. In contrast, three major peaks are observed in chloroform solutions of **1**–**4** (C = 5•10^{-4} M), **5** (C = 1.25•10^{-4} M), **7** and **8** (C = 2.5•10^{-4} M) (Figure 9). Based on the agreement of these peaks with the three lowet excitation energies computed for the dpa dimer (Table 2, last column), we assign the three peaks at 330, 300 and 285 nm to absorption by small soluble aggregates consisting of at least dimers. We recall here that our calculations revealed that the additional absorption peak observed in the dimer is due to a local excitation of a single $(dpaH)^+$ monomer and not an exciton.

To confirm that the additional absorption peaks in the spectra measured in $CHCl_3$ are indeed due to aggregation, as our computations suggest, we diluted the solutions from 5.0•10^{-4} M to 1.0•10^{-4} M and re-measured the absorption spectra. As shown in Figure 10 for **2** (and in Figure S25 in ESI† for **3**) the highest energy peak red-shifts upon dilution, whereas the lowest energy absorption exhibits a blue-shift and the peaks characteristic for the aggregation disappear. Overall, dilution brings the absorption spectrum of **2** in closer agreement with the absorption of **2** in methanol. Based on these observations, we conclude that at a concentration of 5•10^{-4} M, the $(dpaH)^+$ monomers form small soluble aggregates, which split to monomers upon dilution. This suggestion is supported by a rapid decrease of the luminescence intensity of **2** upon dilution from 5.0•10^{-4} M to 1.0•10^{-4} M (Figure 11). Because the absorption and emission of the aggregates in chloroform are different for each salt, we can also conclude that the structure of the aggregates in solution depends on the counter ions, just as in the solid state.

Increasing the viscosity of the alcohol solution increases the emission intensity, as shown in Figure 12. This observation further supports the idea that the radiation-less deactivation channel requires a conformational change of $(dpaH)^+$, which is most efficient a low solvent viscosity. Increasing viscosity, therefore, extends the excited state lifetime and enhances the loss of excited state population through photon emission.

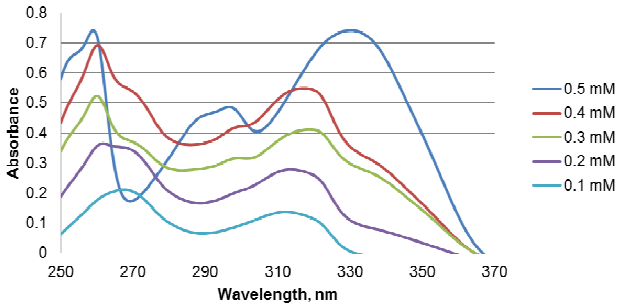

Figure 10. Absorption spectra of 2 in chloroform (C = 1•10^{-4}–5•10^{-4} M).

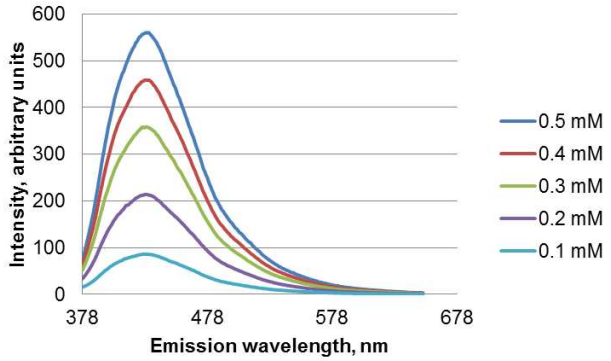

Figure 11. Emission spectra of 2 in chloroform (C = 1•10^{-4}–5•10^{-4} M, λ_{ex} = 368 nm).

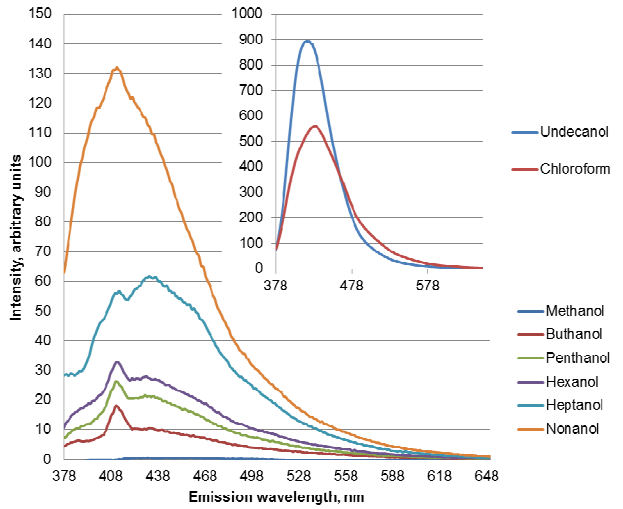

Figure 12. Emission spectra of 2 in the series of alcohols and in chloroform.

Conclusions

We have demonstrated that stacking interactions can induce luminescence in crystals of protonated dpa salts. Our results suggest that the stacking interactions prevent twisting of the pyridyl rings towards the conical intersection, at which radiation-less decay to the ground state would otherwise occur. Therefore, the dpa monomers remain planar and emit instead. Ease of synthesis, commercial availability of the starting materials, and the possibility to tune the optical properties by engineering inter-molecular interactions, could make dpa a versatile building block for constructing OLED devices or sensors.

Acknowledgements

This work was supported by the Academy of Finland through the academy research fellowship to GG. ANC and VYK are indebted to RFBR for grant 13-03-12411-ofim. Financial support provided by the Academy of Finland (project 139571 M. H. and ANC) is also gratefully acknowledged.

Notes and references

[a] Department of Chemistry, University of Jyväskylä, P.O. Box 35, FI-40014 Jyväskylä, Finland

[b] Institute of Chemistry, Saint Petersburg State University, 198504 Stary Petergof, Russian Federation

[c] Nanoscience Center, Univeristy of Jyväskylä, P.O. Box 35, FI-40014 Jyväskylä, Finland

[d] Institute of Photonics, University of Eastern Finland, P.O.Box 111, FI-80101 Joensuu, Finland

† Electronic Supplementary Information (ESI) available: Crystallographic data for **1**–**6** and **8** (CCDC 1004967 – 1004976), absorption maxima of the compounds **1**–**5**, **7**, and **8** in MeOH and CHCl3, geometry of the neutral dpa on ground state and concentration dependent absorption spectra of chloroform solutions of **3**. See DOI: 10.1039/b000000x/

1 D. Li, H. Zhang, Y. Wang, *Chem. Soc. Rev.*, 2013, **42**, 8416.
2 A. C. Grimsdale, K. L. Chan, R. E. Martin, P. G. Jokisz, A. B. Holmes, *Chem. Rev.*, 2009, **109**, 897.
3 S.-C. Lo, P. L. Burn, *Chem. Rev.*, 2007, **107**, 1097.
4 J. G. C. Veinot, T. Marks, *J. Acc. Chem. Res.*, 2005, **38**, 632.
5 S. Wu, M. Aonuma, Q. Zhang, S. Huang, T. Nakagawa, K. Kuwabara, C. Adachi, *J. Mater. Chem. C*, 2014, **2**, 421.
6 X. J. Feng, S. F. Chen, Y. Ni, M. S. Wong, M. M. K. Lam, K. W. Cheah, G. Q. Lai, *Org. Electron.*, 2014, **15**, 57.
7 P. Kotchapradist, N. Prachumrak, R. Tarsang, S. Jungsuttiwong, T. Keawin, T. Sudyoadsuk, V. Promarak, *J. Mater. Chem. C*, 2013, **1**, 4916.
8 D. Volyniuk, V. Cherpak, P. Stakhira, B. Minaev, G. Baryshnikov, M. Chapran, A. Tomkeviciene, J. Keruckas, J. V. Grazulevicius, *J. Phys. Chem. C*, 2013, **117**, 22538.
9 K. Masui, H. Nakanotani, C. Adachi, *Org. Electron.*, 2013, **14**, 2721.
10 W. Wan, H. Du, J. Wang, Y. Le, H. Jiang, H. Chen, S. Zhu, J. Hao, *Dye. Pigment.*, 2013, **96**, 642.
11 S.-W. Wen, M.-T. Lee, C. H. J. Chen, *Disp. Technol.*, 2005, **1**, 90.
12 J. B. Birks, *Photophysics of Aromatic Molecules*; Wiley: London, 1970.
13 D. Bose, G. Mostafa, H.-K. Fun, B. K. Ghosh, *Polyhedron*, 2005, **24**, 747.
14 C. Seward, S. Wang, *Comm. Inorg. Chem.*, 2005, **26**, 103.
15 J. Pang, E. J.-P. Marcotte, C. Seward, R. S. Brown, S. Wang, *Angew. Chem., Int. Ed.* 2001, **40**, 4042.
16 D. P. Segers, M. K. DeArmond, *J. Phys. Chem.*, 1982, **86**, 3768.
17 S. Martić, G. Wu, S. Wang, *Inorg. Chem.* 2008, **47**, 8315.
18 K. Dinakaran, C.-H. Chou, S.-L. Hsu, K.-H. Wei, *J. Polym. Sci. Part A Polym. Chem.*, 2004, **42**, 4838.
19 B. Biswas, S.-P. Hung, H.-L. Tsai, R.Ghosh, N. *J.* Kole, *Coord. Chem.*, 2012, **65**, 2280.
20 D. Bai, S. Wang, *Organometallics*, 2004, **23**, 5958.
21 J. Pang, Y. Tao, S. Freiberg, X.-P. Yang, M. D'Iorio, S. Wang, *J. Mater. Chem.*, 2002, **12**, 206.
22 S. Hotchandani, A. C. Testa, *J. Lumin.*, 1994, **59**, 59.
23 J. H. Lee, H. M. Park, S. P. Jang, G. H. Eom, J. M. Bae, C. Kim; Y. Kim, S.-J. Kim, *Inorg. Chem. Commun.*, 2012, **15**, 212.
24 H. Zhu, M. Ströbele, Z. Yu, Z. Wang, *Inorg. Chem. Commun.*, 2001, ***4***, 577.
25 K.-Y. Ho, W.-Y. Yu, K.-K. Cheung, C.-M. Che, *J. Chem. Soc., Dalt. Trans.*, 1999, **14**, 1581.
26 J. Ashenhurst, L. Brancaleon, S. Gao, W. Liu, H. Schmider, S. Wang, G. Wu, Q. G. Wu, *Organometallics*, 1998, **17**, 5334.
27 S. W. Thomas, G. D. Joly, T. M. Swager, *Chem. Rev.*, 2007, **107**, 1339.
28 Y. Hong, J. W. Y. Lam, B. Z. Tang, *Chem. Soc. Rev.*, 2011, **40**, 5361.
29 Y. Hong, J. W. Y. Lam, B. Z. Tang, *Chem. Commun.*, 2009, **29**, 4332.
30 J. Luo, Z. Xie, J. W. Y. Lam, L. Cheng, B. Z. Tang, H. Chen, C. Qiu, H. S. Kwok, X. Zhan, Y. Liu, D. Zhu, *Chem. Commun.*, 2001, **381**, 1740.
31 CIE 182:2007, *Calibration methods and photoluminescent standards for total radiance factor measurements*; Commission Internationale de L'Eclairage, 2007.
32 P. Turunen, J. Kinnunen, J. Mutanen, *Modeling of Fluorescent Color Mixing by Regression Analysis*; 5th European Conference on Colour in Graphics, Imaging, and Vision- CGIV 2010, Society for Imaging Science and Technology, 2010, pp. 94-100.
33 L. G. Coppel, M. Andersson, P. Edström, *Appl. Opt.*, 2011, **50**, 2784.
34 S. Hamai, F. *J.* Hirayama, *Phys. Chem.*, 1983, **87**, 83.
35 P. C. Junk, L. Wei-Min, L. I. Semenova, B. W. Skelton, A. H. White, *Z. Anorg. Allg. Chem.*, 2006, **632**, 1303.
36 H. Bock, H. Schodel, T. T. H. Van, R. Dienelt, M. Gluth, *J. Prakt. Chem.*, 1998, **340**, 722.
37 Bruker AXS, *APEX2 – Software Suite for Crystallographic Programs*, Bruker AXS, Inc.: Madison, WI, USA, 2009.
38 A. J. M. Duisenberg, L. M. J. Kroon-Batenburg, A. M. M. Schreurs, *J. Appl. Cryst.*, 2003, **36**, 220.
39 W. Otwinowski, Z. Minor, In *Methods in Enzymology, Macromolecular Crystallography, Part A*; C. W. Carter, J. Sweet, Eds.; Academic Press: New York, USA, 1997; pp. 307–326.
40 G. M. Sheldrick, *Acta Cryst.*, 2008, **A64**, 112.
41 L. Palatinus, G. Chapuis, *J. Appl. Cryst.*, 2007, **40**, 786.
42 O. V. Dolomanov, L. J. Bourhis, R. J. Gildea, J. A. K. Howard, H. Puschmann, *J. Appl. Cryst.*, 2009, **42**, 339.
43 G. M. Sheldrick, *SADABS – Bruker AXS scaling and absorption correction*, Bruker AXS, Inc.: Madison, Wisconsin, USA, 2008.
44 G. M. Sheldrick, *SHELXTL*, Bruker AXS, Inc.: Madison, Wisconsin, USA, 2008.
45 J. Emsley, *Chem. Soc. Rev.*, 1980, **9**, 91.

46 G. M. Sheldrick, *CELL_NOW – Indexing program for twinned crystals*, Bruker AXS, Inc.: Madison, Wisconsin, USA, 2008.
47 G. M. Sheldrick, *TWINABS – Bruker AXS scaling for twinned crystals*, Bruker AXS, Inc.: Madison, Wisconsin, USA, 2008.
48 C. Adamo, V. Barone, *J. Chem. Phys.*, 1999, **110**, 6158.
49 A. A. Granovsky, *J. Chem. Phys.*, 2011, **134**, 214113
50 M. Cossi, N. Rega, G. Scalmani, V. Barone, *J. Comput. Chem.*, 2003, **24**, 669.
51 A. A. Granovsky, *Firefly version 8.0.1*, http://classic.chem.msu.su/gran/firefly/index.html, accessed 7 April 2014.
52 M. S. Gordon, M. W. Schmidt, *In Theory and Applications of Computational Chemistry, the first forty years*, C. E. Dykstra, G. Frenking, K. S. Kim, G. E. Scuseria, Eds., Elsevier: Amsterdam, Netherlands, 2005; pp. 1167-1189.
53 X.-H. Ding, Y.-H. Li, S. Wang, X.-A. Li, W. Huang, *J. Mol. Struct.*, 2013, **1051**, 124.
54 P. Giui, V. Bertolasi, V. Ferretti, G. Gilli, *J. Am. Chem. Soc.*, 1994, **3**, 909.
55 V. Bertolasi, P. Gilli, V. Ferretti, G. Gilli, *Chem. - A Eur. J.*, 1996, **2**, 925.
56 G. Gilli, P. Gilli, *J. Mol. Struct.*, 2000, **552**, 1.
57 I. Uçar, A. Bulut, O. Büyükgüngör, *Acta Cryst.*, 2007, **E63**, o3377.
58 H.Schödel, C. Näther, H. Bock, F. Butenschön, *Acta Cryst.*, 1996, **B52**, 842.
59 N. J. Turro, V. Ramamurthy, J. C. Scaiano, *Principles of Molecular Photochemistry: An Introduction*; University Science Books: Sausalito, CA, 2009; pp. 253–257.
60 J. R. Roscioli, L. R. McCunn, M. A. Johnson, *Science*, 2007, **316**, 249.
61 W. W. Cleland, M. M. Kreevoy, *Science*, 1994, **264**, 1887.
62 N. Zhao, J. W. Y. Lam, H. H. Y. Sung, H. M. Su, I. D. Williams, K. S. Wong, B. Z. Tang, *Chem . Eur. J.*, 2014, **20**, 133